Mechanisms in non-heme iron oxidation catalysis

Chen, Juan

CHAPTER 2

Direct photochemical activation of non-heme Fe(IV)=O complexes

Near-UV excitation of non-heme Fe^{IV}=O complexes results in light intensity dependent increase in reaction rates for the oxidation of C–H bonds even at low temperature (-30 ^{o}C). The enhancement of activity is ascribed to the ligand-to-[Fe^{IV}=O] charge transfer character of the near-UV bands to generate a highly reactive [(L^{+})Fe^{III}-O*] species. The enhancement is not observed with visible/NIR excitation of the d-d absorption bands.

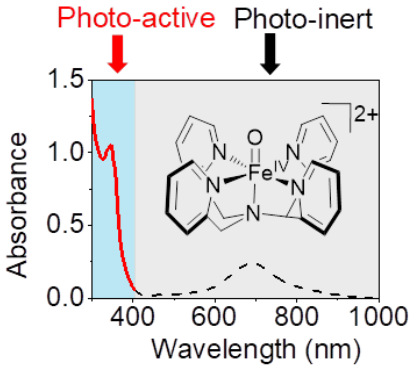

This chapter has been published:

Juan Chen, Apparao Draksharapu, Emma Harvey, Waqas Rasheed, Lawrence Que, Jr. and Wesley R. Browne, *Chem. Commun.* 2017, *53* (91), 12357–12360.

2.1 Introduction

The photochemistry of iron complexes saw a spurt of interest in the 1960s,[1–3] but this interest was rapidly superseded by the photochemistry of Ru(II) complexes, of which the paradigm is $[Ru(bpy)_3]^{2+}$, due to the latter's long lived excited states and luminescence.[1] Indeed the photochemistry of these complexes has seen recent further interest in photoredox catalysis, driven largely by the access they provide to novel SOMO reactivity and, to a lesser extent, in inorganic oxidation catalysis by the possibility of generating reactive intermediates directly without the use of terminal oxidants such as mCPBA, PhIO, H_2O_2 *etc*. $[Ru(bpy)_3]^{2+}$ has been employed as a photo-oxidant to generate high-valent metal-oxido species that can engage in selective oxidation of C–H and C=C bonds. In 2011, Fukuzumi, Nam and co-workers reported the first example of photocatalytic formation of $[(N4Py)Fe^{IV}=O]^{2+}$ (**1**)[4] from step-wise electron transfer oxidation of $[(N4Py)Fe^{II}(CH_3CN)]^{2+}$ (**1a**) by visible light generated photo-excited Ru(II) complexes.[5,6] The C–H oxidation carried out *in situ* by hydrogen atom abstraction (HAT) with **1** is the rate determining step, which places an upper limit to the overall efficiency of the system.[7,8] It is notable, however, that complexes such as $[(N4Py)Fe^{II}(CH_3CN)]^{2+}$ (**1a**) undergo oxidation to their corresponding Fe(III) complexes (**1b**) upon irradiation in water or in methanol.[9] Hence, the photo redox behaviour of iron complexes in general deserves attention also in the context of light-driven oxidation chemistry.

Here we report the wavelength-dependent direct photochemical activation of a series of non-heme iron(IV)-oxo complexes $[(N4Py)Fe^{IV}=O]^{2+}$ (**1**),[4] $[(MeN4Py)Fe^{IV}=O]^{2+}$ (**2**), and $[(Bn\text{-}TPEN)Fe^{IV}=O]^{2+}$ (**3**) (**Figure 21**)[‡] in the absence and presence of oxidisable substrates, both in acetonitrile and in methanol. Although excitation into the NIR absorption bands of complexes **1 - 3** has no discernible effect on the reactivity of these complexes, excitation into near-UV charge transfer bands results in a light-intensity-dependent enhancement of the oxidative reactivity of these complexes towards C–H bonds.

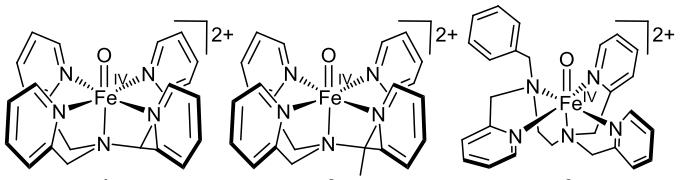

Figure 21. Structures of FeIV=O complexes discussed in the text.

2.2 Results and Discussion

The self-decay of **1** to **1a** in the dark in acetonitrile is negligible over 1 h at 21 °C (5.8×10^{-5} s^{-1}), in accordance with earlier reports.[7] Irradiation of **1** in acetonitrile at 365 nm (**Figure 22**), however, results in a decrease in absorbance at 696 nm, the rate of which is dependent on light intensity (with an overall quantum yield of > 0.006, **Figure 23**). The loss in absorbance at 696 nm is followed, after a delay, by an increase in absorbance at 378 and 454 nm, corresponding to formation of the Fe(II) complex $[(N4Py)Fe^{II}(CH_3CN)]^{2+}$ (**1a**). Comparison with an independently prepared solution of **1a** (**Figure 24**) confirms >95% overall conversion to **1a** and that reduction of **1** does not result in ligand degradation. The rate of photoreduction of **1** in acetonitrile is not obviously affected by the presence or absence of dioxygen (**Figure 25**), nor is it affected by solvent deuteration (CD_3CN, **Figure 25**).

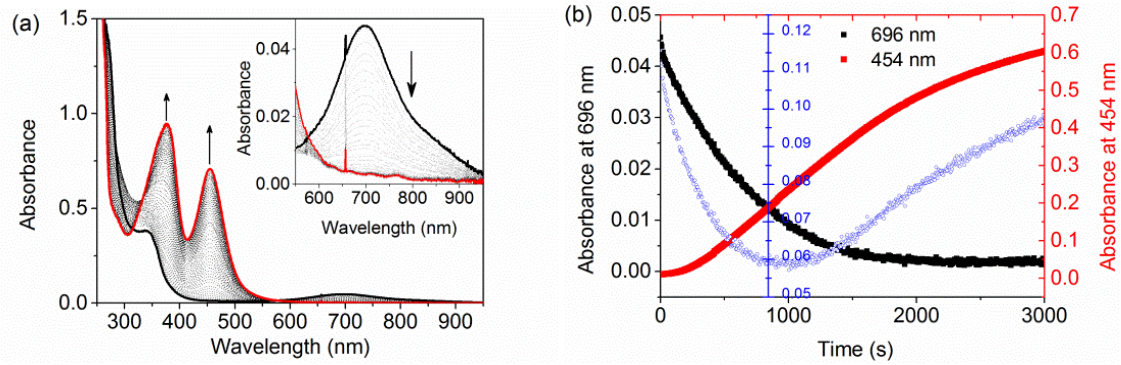

Figure 22. (a) UV-vis absorption spectrum of **1** (0.125 mM) in acetonitrile at 21 °C before (black) and during irradiation at 365 nm (dashed lines) with the final spectrum in red. Inset: expansion from 550 to 950 nm. (b) Absorbance at 696 nm (black, left y-axis) and 454 nm (red, right y-axis) over time. The total concentration of **1** (Fe^{IV}=O) and **1a** ($Fe^{II}(CH_3CN)$) (blue, centred y-axis), was calculated from the absorbance at 696 nm ($\varepsilon_{696\ nm}$ **1** = 400 M^{-1} cm^{-1}) and at 454 nm ($\varepsilon_{454\ nm}$ **1a** = 6520 M^{-1} cm^{-1}).[10]

The total concentration (**1** + **1a**, **Figure 22**, blue trace) calculated from the absorbance at 696 nm and 454 nm (where the spectra of **1** and **1a** show negligible overlap) shows an initial rapid decrease (within 900 s) followed by a slower increase. These data indicate that the photoreduction from the Fe(IV) to the Fe(II) redox state is a multi-step process (**Scheme 3**). The intermediate species formed (*i.e.* the Fe(III) complex, **1b**) do not show significant visible absorption, which is consistent with the lack of an isosbestic point throughout the irradiation. Furthermore, the initial increase and subsequent decrease in absorbance at 310 nm, shown in **Figure 22**a is consistent with the intermediacy of **1b**.

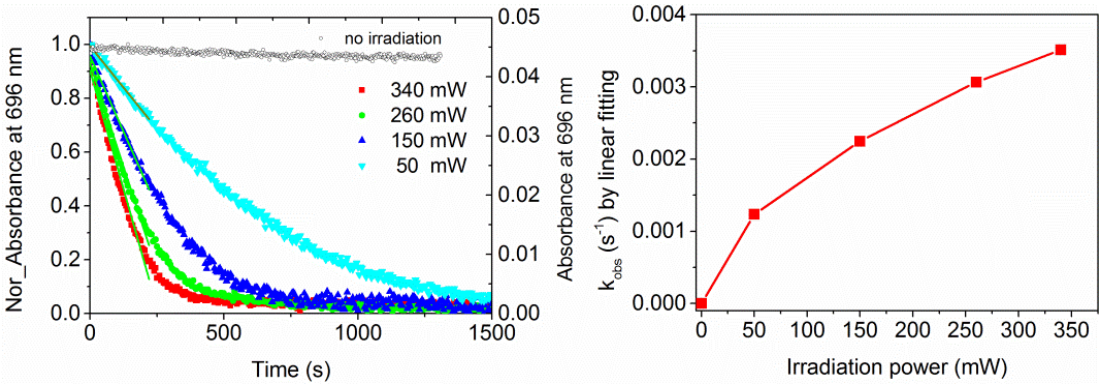

Figure 23. (left) Absorbance at 696 nm of **1** (0.125 mM) in acetonitrile in dark and under irradiation (λ_{exc} = 365 nm) at 21 °C with light intensities of 340 mW (red), 260 mW (green), 150 mW (blue), 50 mW (cyan), (left axis normalized absorbance, right axis actual absorbance). (right) Dependence of k_{obs} value on irradiation power obtained by linear fitting (green lines in left graph) of the first 250 s of the decay.

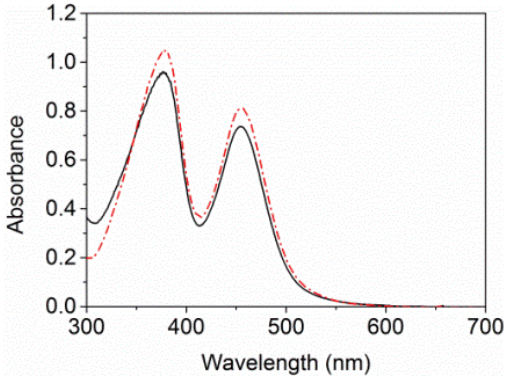

Figure 24. UV-vis absorption spectra of the photo product (λ_{exc} = 365 nm) of **1** (0.125 mM, black) in acetonitrile with **1a** (0.125 mM, red) in acetonitrile.

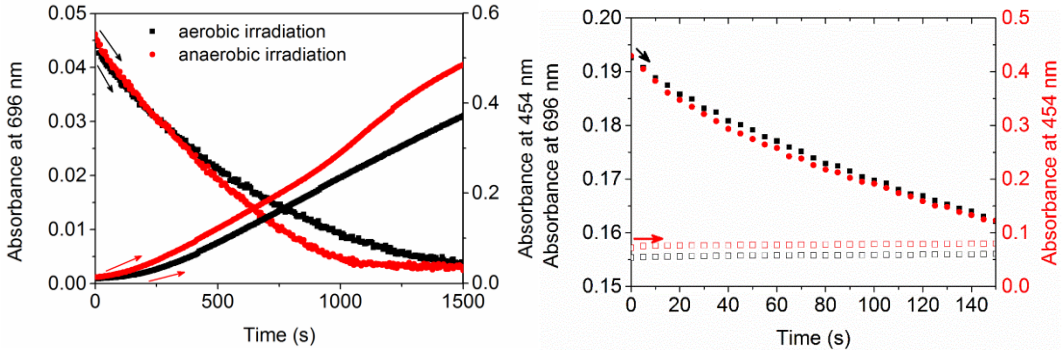

Figure 25. (left) Absorbance at 454 nm (red arrow, right y-axis) and at 696 nm (black arrow, left y-axis) with **1** (0.125 mM) in acetonitrile over time during irradiation at 365 nm under aerobic (black) and anaerobic (red) conditions at 21 °C. (right) Absorbance at 454 nm (red arrow, right y-axis) and at 696 nm (black arrow, left y-axis) with **1** (0.5 mM) in CH_3CN (black) over time with irradiation at 365 nm and CD_3CN (red), at 21 °C.

EPR spectra (**Figure 26**) show that the initial decrease of **1** results in the formation of primarily one low-spin Fe^{III} species, $[(N4Py)Fe^{III}\text{-}X]^{2+}$ (g = 2.29, 2.12, 1.96), as well as a minor amounts of low-spin $[(N4Py)Fe^{III}\text{-}OH]^{2+}$ (g = 2.41, 2.16, 1.92) and high-spin $[(N4Py)Fe^{III}\text{-}OH_2]^{3+}$ (g = 4.3). Double integration and comparison with the spectrum of the low-spin Fe^{III} species **1b**, shows that the decrease in concentration of **1** in acetonitrile is approximately equal to the increase in concentration of a low-spin Fe^{III} species and the Fe^{II} complex **1a**.

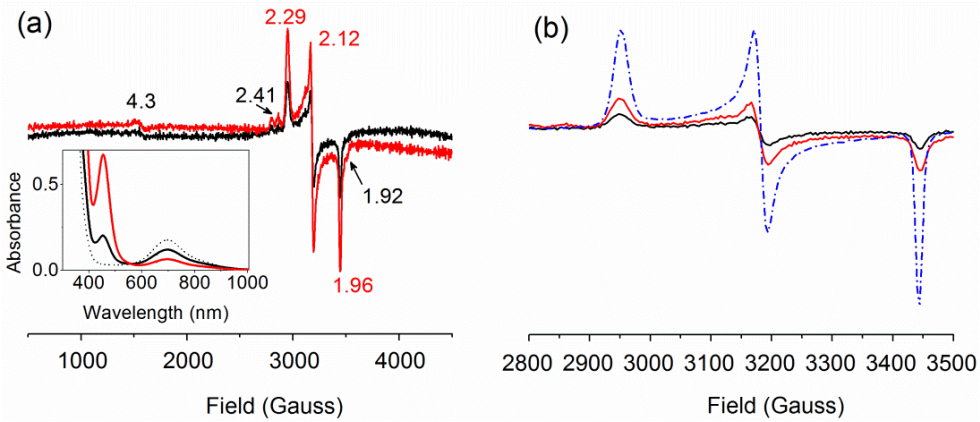

Figure 26. (a) X-band EPR (77 K) spectra of **1** (0.5 mM) in acetonitrile under irradiation 365 nm; sample was flash frozen at ca. 30% (black, double integration (spins) = 2.332×10^8) and at 66%

(red, double integration = 4.565 × 10^8) photo-reduction of **1** at 21 °C. Inset shows the corresponding UV-vis absorption spectra. (b) Expansion of the 2800 - 3500 G range, and comparison with a 0.5 mM solution of $[(N4Py)Fe^{III}(OCH_3)]^{2+}$ (in blue, double integration = 8.262 × 10^8). Considering the formation of Fe^{II} (~ 0.1 mM, calculated from the absorbance at 454 nm ($\varepsilon_{454\ nm}$ **1a** = 6520 M^{-1} cm^{-1})), it can be concluded that the loss of **1** (0.5 mM × 66% = 0.33 mM) was due to the formation of Fe^{III} (~ 0.27 mM) and Fe^{II} (~ 0.1 mM) complexes.

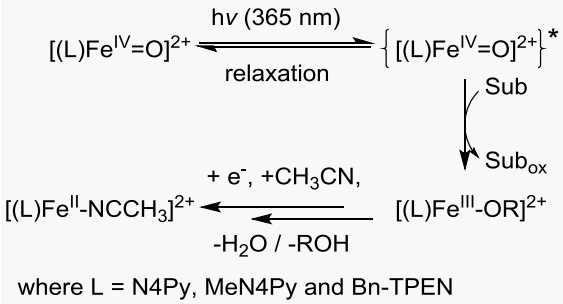

Scheme 3. Initial reaction of photo-excited Fe(IV)=O complexes results in thermal relaxation or reduction to their Fe(III)-OR analogues (R = H, alkyl), which undergoes subsequent slower reduction together with ligand exchange to form, *e.g.,* **1a**.

The structurally related Fe^{IV}=O complex **2** ($[(MeN4Py)Fe^{IV}=O]^{2+}$) shows a similar effect of irradiation as seen for **1** (**Figure 27** and **Figure 28**).[§] In contrast to **1** and **2**, for $[(BnTPEN)Fe^{IV}=O]^{2+}$ (**3**) a nearly linear decrease in absorbance at 740 nm and concomitant increase in absorbance of an Fe^{II} species at 388 nm are observed, indicating that the second step (Fe^{III} to Fe^{II}) is rapid (**Figure 29**).[7] Similar with that in **1**, the rate of reduction of **3** is also dependent on the irradiation intensity (**Figure 30**).

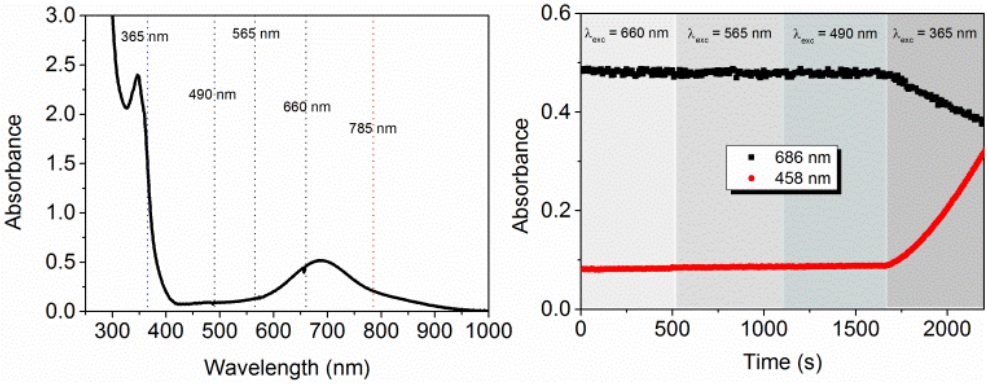

Figure 27. (a) UV-vis absorption spectrum of **2** (1 mM) in acetonitrile at 21 °C. (b) The corresponding change in absorbance at 686 nm (black) and 458 nm (red) under irradiation at various wavelengths. Irradiation by 785 nm (100 mW) has no effect on the spectrum compared to a non-irradiated samples over 3 h. Slope with irradiation at 660, 565 and 490 nm is 2.7 x 10^{-6} s^{-1} and with irradiation at 365 nm is 1.6 x 10^{-4} s^{-1}

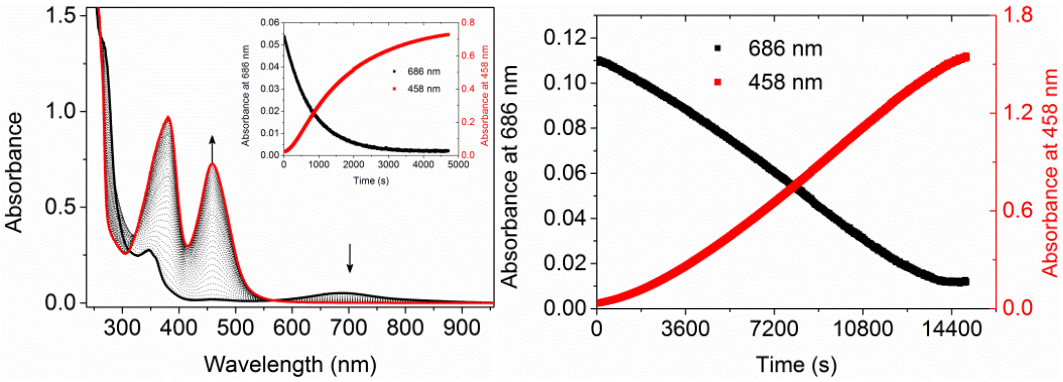

Figure 28. (left) UV-vis absorption spectrum of **2** (0.125 mM) in acetonitrile before (black) and during irradiation at 365 nm (dashed lines) with the final spectrum in red. Inset: absorbance at 686 nm (black, left y-axis) and 458 nm (red, right y-axis) over time at 21 °C. (right) Absorbance at 458 nm and at 686 nm with **2** (0.125 mM) in acetonitrile over time under irradiation at 300 nm at 21 °C.

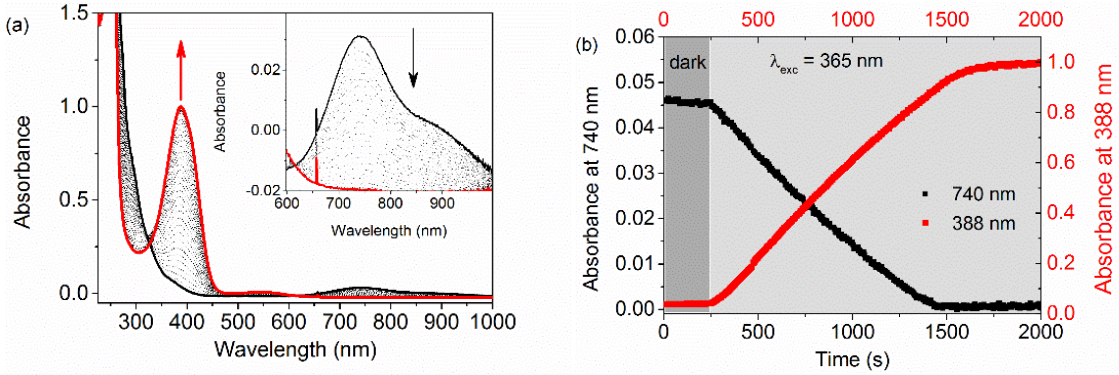

Figure 29. (a) UV-vis absorption spectrum of **3** (0.125 mM) in acetonitrile at 21 °C before (black) and during irradiation at 365 nm (dashed lines) with the final spectrum in red. Inset: expansion from 600 to 1000 nm. (b) Absorbance at 740 nm (black, left y-axis) and 388 nm (red, right y-axis) upon irradiation being initiated at 250 s. The slope without irradiation (dark grey stage) is 3.0×10^{-6} s^{-1} and 4.5×10^{-5} s^{-1} with irradiation (light grey stage).

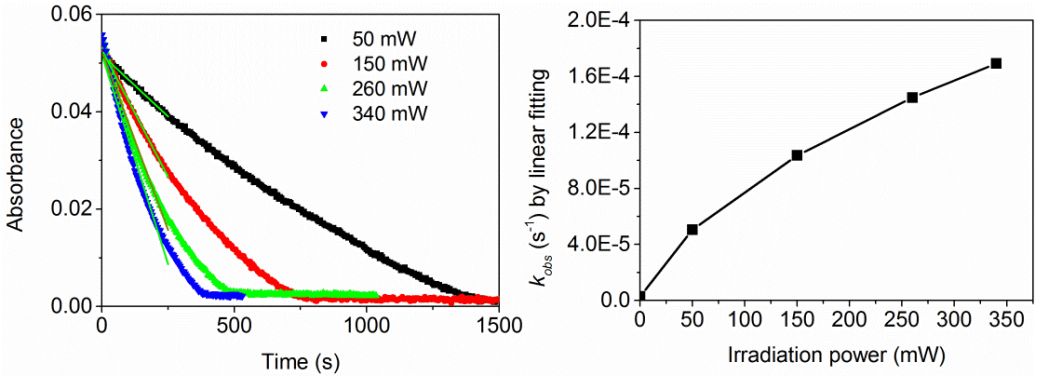

Figure 30. (left) change in absorbance at 740 nm of **3** (0.125 mM) in acetonitrile under irradiation (λ_{exc} = 365 nm) at 21 °C at 50 mW (black), 150 mW (red), 260 mW (green), 340 mW (blue) at 21 °C. (right) Dependence of k_{obs} obtained by linear fitting of the first 250 s of the decay (green lines in left graph) with irradiation power.

The photoinduced reduction shows a pronounced wavelength dependence. For example, even prolonged intense irradiation (at 490, 565, 660 and 785 nm) into the d-d absorption bands of **2** shows no effect (**Figure 27**), in contrast to the photoinduced reduction observed upon irradiation into the LMCT bands (365 and 300 nm, **Figure 28**).

The oxidation of C–H bonds by complexes such as **1 - 3** has been studied in detail and the thermal reaction is generally accepted to proceed via a HAT mechanism, with HAT as the rate determining step.[7,11] At 21 °C, **1** oxidizes substrates such as benzyl alcohol (**BA**), and ethylbenzene (**EB**), with the later oxidized at a ca. 10 times lower rate than the former (**Figure 31** and **Table 2**). In the presence of either substrate (*i.e.* 5 equiv **BA** or 50 equiv of **EB**), irradiation in acetonitrile at 21 °C results in a four-fold increase in the rate of decrease in the NIR absorbance of **1** compared to the thermal reaction and two fold increase (with **BA**) compared to irradiation of **1** in acetonitrile alone (**Table 2**). Notably, the near 10 fold increase in the rate of increase in visible absorbance of **1a** under photo-irradiation in the presence of **BA** indicates that the observed reaction rate is dominated by photokinetics (**Table 2**). The oxidation of **BA** and **EB** under irradiation was confirmed by GC-MS analysis of the reaction mixtures.

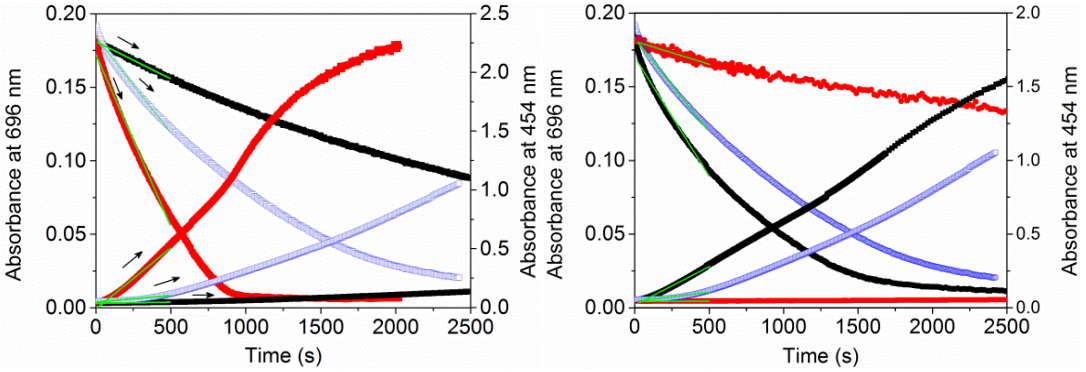

Figure 31. Absorbance at 696 nm (decrease over time, left-axis) of **1** (0.5 mM) and absorbance at 454 nm (increase with time, right axis) in the presence of (left) 5 equiv benzyl alcohol (**BA**) and (right) 50 equiv ethylbenzene (**EB**) in CH_3CN at 21 °C with (red, λ_{exc} = 365 nm) and without irradiation (black). The changes in absorbance in the absence of substrate (**BA** and **EB**) are shown in blue. The slopes obtained from linear fitting of the first 500 s (green lines) are summarized in **Table 2**.

Table 2. Comparison of the rate of the change of **1** under irradiation and in the dark at 21 °C with and without ethylbenzene or benzyl alcohol.

	substrates	Rate of decrease in absorbance of Fe^{IV}=O ($\times 10^{-5}$ s^{-1})[a]	Rate of increase in absorbance of Fe^{II} ($\times 10^{-4}$ s^{-1})[b]
Under irradiation	5 equiv BA ($C_6H_5CH_2OH$)	23	10
	50 equiv EB ($C_6H_5C_2H_5$)	16	5.2
	CH_3CN only	12	1.1
In Dark	5 equiv BA ($C_6H_5CH_2OH$)	5.1	0.17
	50 equiv EB ($C_6H_5C_2H_5$)	3.1	0.03
	CH_3CN only	<0.001	<0.001

Values are obtained by linear fitting the changes of the absorbance at 696 nm[a] and 454 nm[b] for the first 500 s of the reaction.

At -30 °C, the rate of the thermal reaction of **1** with **BA** is reduced substantially[11] even with 50 equiv with respect to **1** (second order rate constant is ca. 2.3 x 10^{-6} M^{-1} s^{-1}, **Figure 32** and **Figure 33**). In contrast, the rate of reduction of **1** under irradiation is not affected significantly by the decrease in temperature (**Table 3**). Furthermore, although the thermal reaction shows the expected dependence on the concentration of **BA**, the k_{obs} under irradiation is much less sensitive to substrate concentration (**Table 3**). Cyclohexanol, which has stronger C-H bonds than **BA**, shows a similar influence on the rate of decay of **1** under irradiation (**Figure 34**, **Table 4**).

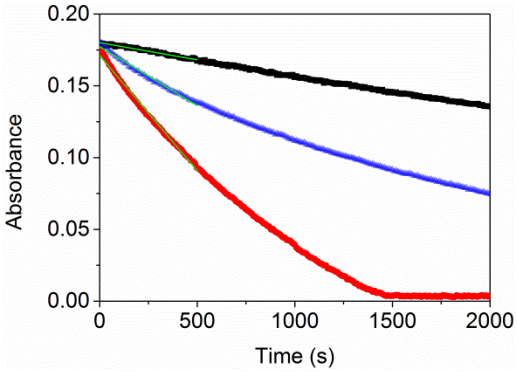

Figure 32. Absorbance at 696 nm over time of **1** (0.5 mM) in acetonitrile at -30 °C: (black) with 50 equiv **BA**, (blue) under irradiation (365 nm) without **BA**, and (red) under irradiation (365 nm) with **BA**. Linear fitting of the first 500 s shown as green lines, slope for thermal reaction is 2.4 x 10^{-5} s^{-1}, and for photoreaction with **BA** is 1.6 x 10^{-4} s^{-1}, and without **BA** is 0.8 x 10^{-4} s^{-1}.

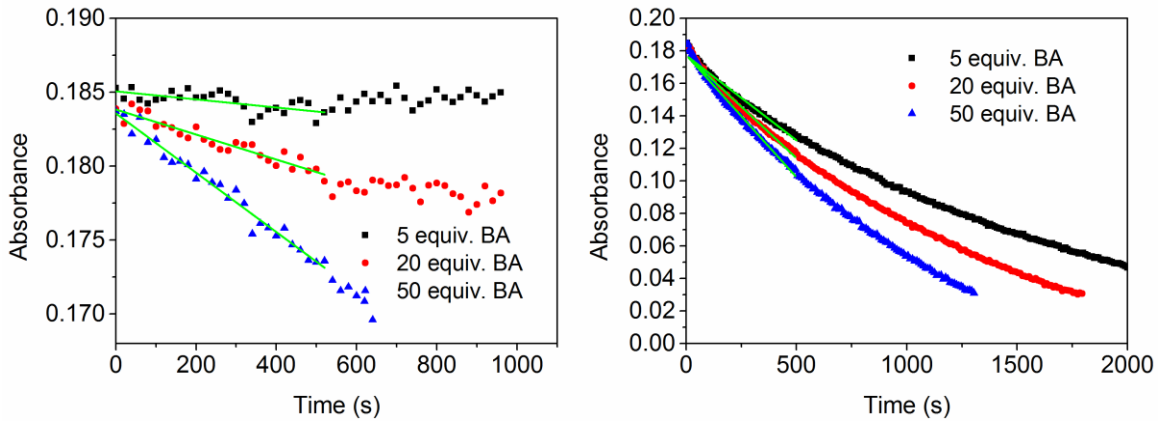

Figure 33. Absorbance at 696 nm of **1** (0.5 mM) in acetonitrile over time in the presence of 5, 20 and 50 equiv **BA** in the dark (left) and under irradiation at 365 nm (right) at -30 °C. Green lines show linear fitting over the first 500 s are summarized in **Table 3**.

Table 3. Observed rate of change in absorbance at 696 nm of **1** under irradiation and dark in the presence of benzyl alcohol (**BA**) at -30 °C.

Substrate equiv w.r.t **1**	Under irradiation (× 10^{-4} s^{-1})	In Dark ((× 10^{-6} s^{-1})
5 equiv	1.0	2.7
20 equiv	1.3	8.5
50 equiv	1.5	20

Values are obtained by linear fitting the decrease of the absorbance at 696 nm for the first 500 s of the reaction

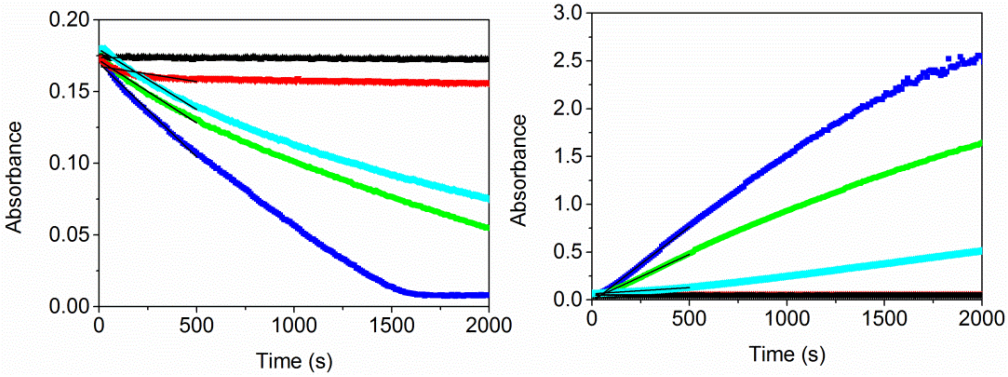

Figure 34. Absorbance at 696 nm (left) and at 454 nm (right) over time with of **1** (0.5 mM) in acetonitrile at -30 °C. In dark: with 50 equiv cyclohexanol-H_{12} (red), 50 equiv cyclohexanol-D_{12} (black); Under irradiation at 365 nm: in absence of cyclohexanol (cyan), and with 50 equiv cyclohexanol-H_{12} (blue), and with 50 equiv cyclohexanol-D_{12} (green). Black lines indicate the linear fitting of the changes over the first 500 s, see **Table 4** for data.

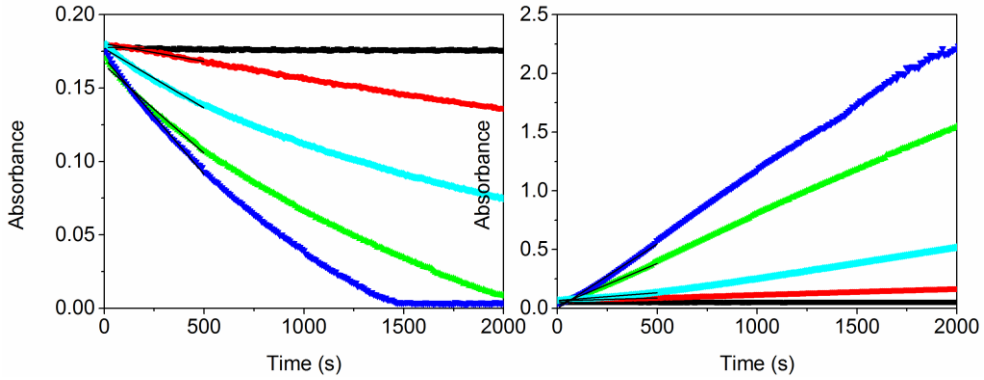

Figure 35. Absorbance at 696 nm (left) and at 454 nm (right) over time with of **1** (0.5 mM) in acetonitrile at -30 °C. In dark; with 50 equiv benzyl alcohol-α,α-H_2 (red), benzyl alcohol-α,α-D_2 (black); Under irradiation at 365 nm in absence of benzyl alcohol (cyan); and with 50 equiv benzyl alcohol-α,α-H_2 (blue), and with 50 equiv benzyl alcohol-α,α-D_2 (green). Black lines indicate the linear fitting of the changes over the first 500 s, see **Table 4** for data.

Overall the data indicate that, in contrast to the thermal reaction, the overall photochemical reaction rate is dominated by irradiation intensity (*i.e.*, photokinetics). The reaction between **1*** (*i.e.*, **1** in its electronically excited state, **Scheme 4**) and the substrate competes with non-radiative relaxation to **1**, which is the dominant relaxation pathway. Furthermore, the rate of oxidation of **BA** and cyclohexanol (k_2), although less than thermal relaxation (k_{-1}), is greater than the rate of oxidation of solvent or **EB** (k_3). The photokinetic control (*i.e.*, balance of k_1 and k_{-1}) also rationalises the relatively modest observed effect of deuteriation in the case of both cyclohexanol and **BA** (**Figure 34** and **Figure 35**), which leads to an underestimation KIE (kinetic isotope effect) for the reaction of **1*** with the alcohol (**Scheme 4**). Analysis of the product mixture obtained from irradiation of a 1:1 mixture of benzyl alcohol and 1,1-D_2-benzylalcohol indicates that the KIE is ca. 1.5 (**Figure 36**), in agreement with the KIE obtained by a comparison of rates.

Table 4. Comparison of the rate of change in absorbance of **1** under irradiation and in dark in acetonitrile at -30 °C with and without 50 equiv cyclohexanol or benzyl alcohol (**BA**) present.

	substrates	Rate of decrease in absorbance of Fe^{IV}=O (× 10^{-5} s^{-1})[a]	Rate of increase in absorbance of Fe^{II} (× 10^{-4} s^{-1})[b]
Under irradiation	benzyl alcohol-α,α-D_2	12	7.2
	benzyl alcohol-α,α-H_2	16	11
	cyclohexanol-D_{12}	8.7	9.4
	cyclohexanol-H_{12}	13	16
	No alcohol present	8.1	1.3
In dark	benzyl alcohol-α,α-D_2	0.36	0.018
	benzyl alcohol-α,α-H_2	2.4	0.505
	cyclohexanol-D_{12}	0.009	<0.001
	cyclohexanol-H_{12}	2.1	0.005
	No alcohol present	< 0.01	< 0.001

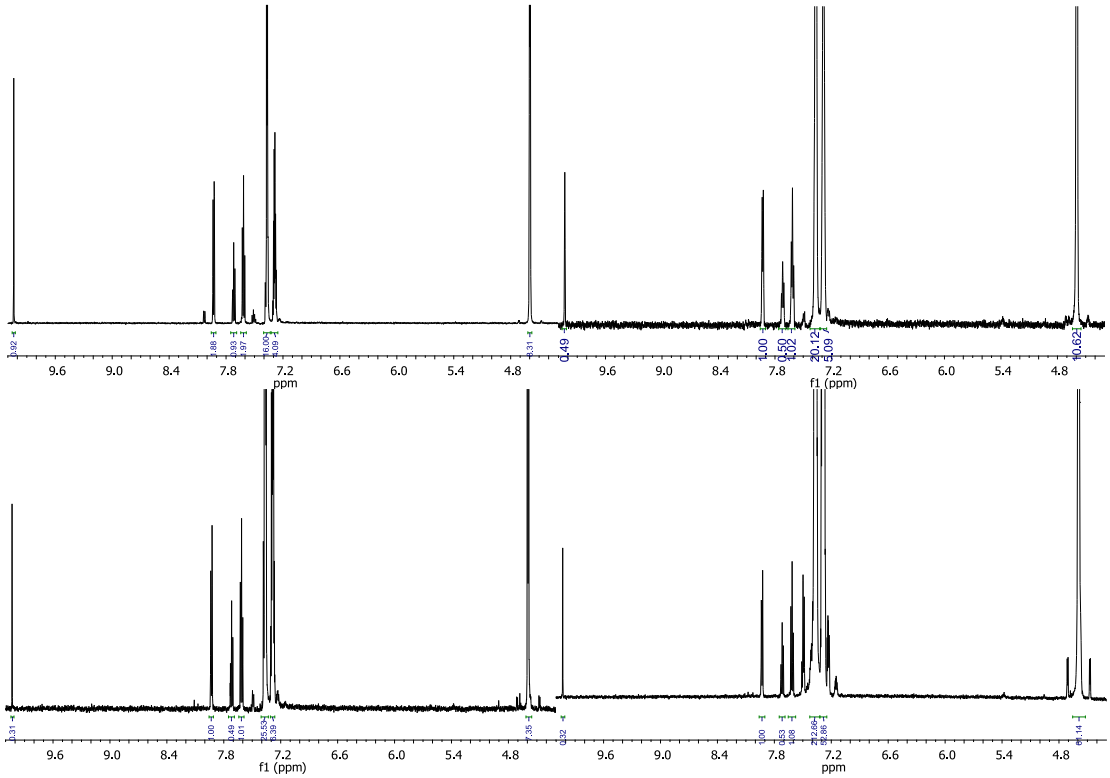

Figure 36. ^{1}H NMR (600 MHz) spectra in CD_3CN of: (top left) a mixture of benzyl alcohol and benzaldehyde (4:1), (top right) benzyl alcohol (2.5 mM) with **1** (0.5 mM) after irradiation at 365 nm, (bottom left) benzyl alcohol (1.25 mM) and 1,1-D_2-benzyl alcohol (1.25 mM) and with **1** (0.5 mM) after irradiation at 365 nm, and (bottom right) benzyl alcohol (12.5 mM) and 1,1-D_2-benzyl alcohol (12.5 mM) and with **1** (0.5 mM) after irradiation at 365 nm. In each case, the irradiation was carried out in a 1 cm quartz cuvette with monitoring by UV/Vis absorption spectroscopy. Irradiation was stopped at the point that the absorbance at 696 nm reached zero, 1 ml of the solution was passed through a plug of silica to remove **1a** and the ^{1}H NMR spectra were recorded.

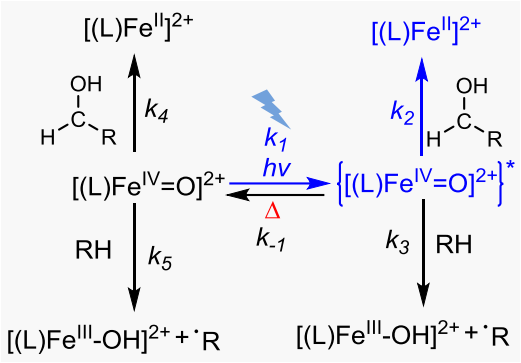

Scheme 4. Proposed mechanism for photo-activation of **1** towards to the substrates oxidation

In methanol,[§§] the effect of near-UV irradiation on **1** (**Figure 37** and **Figure 38**) is readily apparent with an estimated quantum efficiency of ca. 0.14, at -30 °C solvent deuteration has no effect on the rate of reduction of **1** (CH_3OH vs. CD_3OD, **Figure 39**). The primary photo product at room temperature is the low-spin Fe^{III} complex $[(N4Py)Fe^{III}\text{-}OCH_3]^{2+}$ (X-band EPR at 77 K, g = 2.29, 2.12, 1.96).[12] That the final oxidation state is Fe^{III} and not Fe^{II}, as is the case in acetonitrile, is expected given the large (ca. 0.6 V) difference in the Fe^{III}/Fe^{II} redox potentials of the methanol and acetonitrile bound complexes.

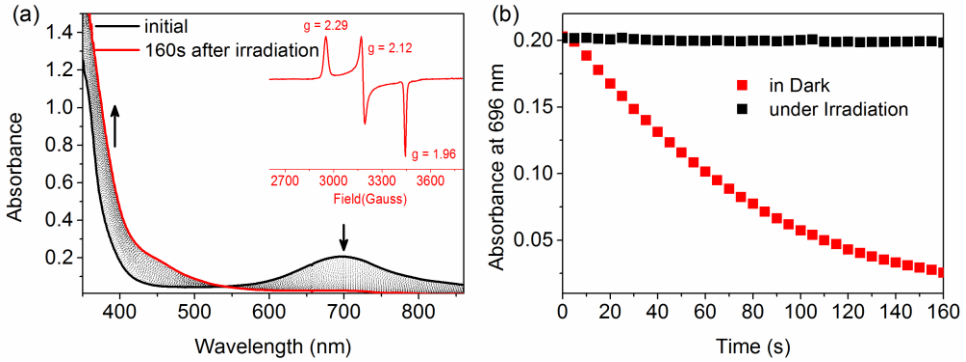

Figure 37. (a) UV-vis absorption spectrum of **1** (0.5 mM) in CD_3OD at 20 °C before (black) and during (dashed lines) irradiation at 365 nm; final spectrum (red). Inset: X-band EPR spectrum of flash frozen solution at 77 K. (b) Absorbance at 692 nm of **1** over time without (black, initial slope 4.9×10^{-5} s^{-1}) and with irradiation (red, initial slope 1.9×10^{-3} s^{-1}).

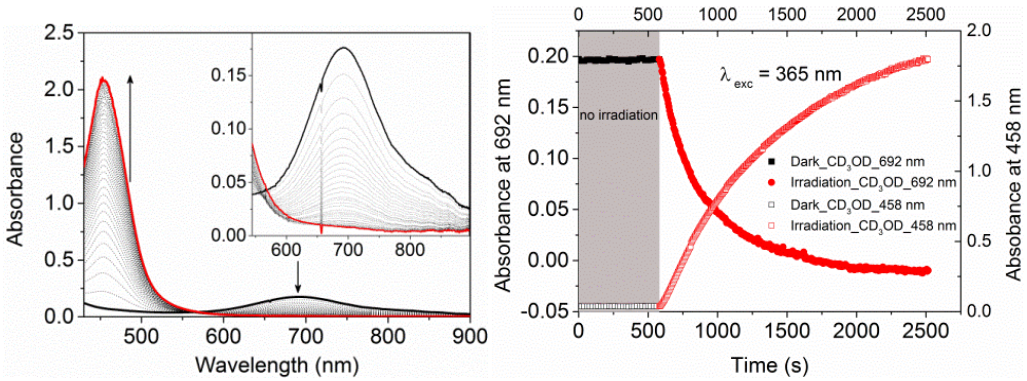

Figure 38. (left) UV-vis absorption spectrum of **1** (0.5 mM) in CH_3OH at -30 °C before (black) and during irradiation at 365 nm (dashed lines) with the final spectrum in red. Inset is the expansion at range 500 to 900 nm. (Right) the corresponding absorbance at 692 nm (solid squares, left y-axis) and 458 nm (open squares, right y-axis) over time. Irradiation was commenced at 600 s.

At -30 °C, disproportionation is supressed and the Fe^{II} complex forms concomitant with the decrease in the absorbance of **1**. Oxidation of methanol to methanal under photo-irradiation proceeds with ca. 64% efficiency (determined colorimetrically, 0.32 equiv CH_2O w.r.t to **1**).

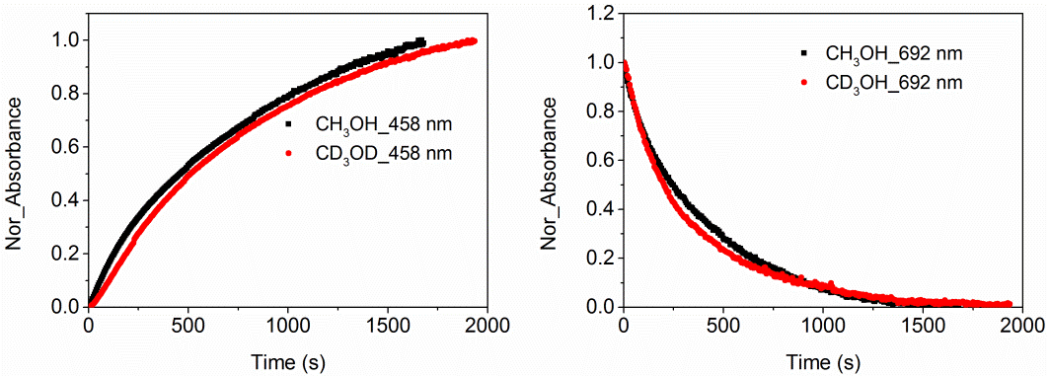

Figure 39. Comparison of normalized absorbance of **1** (0.5 mM) at 458 nm (left) and 692 nm (right) in CH_3OH (black) and in CD_3OD (red) over time at -30 °C during irradiation at 365 nm.

The various reactions of importance in the photo-activation of **1** towards substrate oxidation are shown in **Scheme 4**. The overall rate of decay in the absorbance of **1** (or **2**, **3**) in acetonitrile is determined by photon flux, i.e. k_1, and the concentration of **1*** is limited by a combination of non-radiative relaxation of the excited state (k_{-1}) as well as the rate constants for reaction with oxidizable substrates (k_3 and k_5). Although reaction with alcohols proceeds more rapidly than with acetonitrile (i.e. $k_2 >> k_3$), the overall rate of reaction is dominated by k_1/k_{-1}. In the presence of, for example, benzyl alcohol, the reaction goes primarily via oxidation of the alcohol (manifested in the concomitant formation of the **1a**), the extent of the background reaction with acetonitrile is reduced by the decrease in the excited state lifetime of **1***.

Most reported Fe^{IV}=O complexes have S = 1 ground states with a strong Fe=O double bond character (bond distance ca. 1.65 Å).[13] Their reactivity towards substrates depends strongly on their ligand environments, with $[(N4Py)Fe^{IV}=O]^{2+}$ (**1** in **Figure 21**) and $[(Bn\text{-}TPEN)Fe^{IV}=O]^{2+}$ (**3**) showing surprising stability but nevertheless engaging in C–H bond oxidation, including oxidizing cyclohexane at room temperature.[7] The excited state reached upon visible-NIR excitation is shown, in the present study, not to lead to reduction of **1** nor C–H bond oxidation. In contrast, excitation into the more intense near-UV LMCT bands results in photoinduced reduction. The absorption spectrum of **1** has been characterised earlier by Solomon and co-workers in detail by magnetic circular dichroism (MCD) spectroscopy coupled with DFT calculations.[14] The NIR bands of **1** between 580 to 900 nm are assigned to mixing of formally forbidden $d_{(x^2-y^2)} \leftarrow d_{(xz/yz)}$ transitions with ligand(oxido)-to-metal charge-transfer (LMCT) (from the equatorial nitrogens to the $d_{(x^2-y^2)}$ orbital) transitions. The near-UV band was assigned as a LMCT band with charge transferred from the pyridine π MOs to the Fe-O π* orbitals ($d_{(xz/yz)} \leftarrow \pi_{pyr}$ charge transfer), resulting in a weakening and hence elongation of the Fe(IV)=O bond and an increase in its oxyl radical character, making it a more powerful C–H bond abstracting agent.

2.3 Conclusions

In conclusion, we have shown that near-UV excitation of a series of non-heme Fe^{IV}=O complexes results in a dramatic enhancement of their reactivity towards C–H activation. The decay kinetics and wavelength dependence indicate strongly that it is a relatively long lived (0.1 to

5 ns)[15] LMCT state that is involved and not the d-d excited states accessed by visible excitation. In light of the emergence of the field of photoredox catalysis and especially the use of Ru(II) polypyridyl complexes as photo-oxidants to generate Fe^{IV}=O species in solution,[6] the present study raises the possibility that the initially formed Fe^{IV}=O species (*e.g.,* **1**) is in fact formed as **1*** and hence the intrinsic reactivity may be different from that expected for ex situ prepared **1**. Furthermore, the use of near-UV light opens the possibility to directly enhance the reactivity of such complexes.

2.4 Experimental section

Synthesis. The ligand 1,1-di(pyridin-2-yl)-N,N-bis(pyridin-2-ylmethyl)methanamine (N4Py),[16] 1,1-di(pyridin-2-yl)-N,N-bis(pyridin-2-ylmethyl)ethan-1-amine (MeN4Py),[10] $[(N4Py)Fe^{II}(CH_3CN)](ClO_4)_2$ (**1a**),[10] $[(MeN4Py)Fe^{II}(CH_3CN)](ClO_4)_2$ (**2a**), and $[(Bn\text{-}TPEN)Fe^{II}(OTf)](OTf)$ (**3a**)[7] were prepared as reported previously. Commercially available chemicals were purchased from Sigma Aldrich without further purification. All solvents used for spectroscopy were of UVASOL (Merck) grade.

$[(N4Py)Fe^{IV}(O)](PF_6)_2$ (1). Cerium ammonium nitrate (CAN) (208 mg, 0.38 mmol) in water (0.3 mL) was added to $[(N4Py)Fe^{II}(Cl)](Cl)$ (85.3 mg, 0.17 mmol) in acetonitrile/water (1:1 v/v, 3.5 mL). A blue solid crashed out of the solution upon addition of aqueous KPF_6 (210 mg, 1.15 mmol in 2 mL water). The precipitate was recovered by vacuum filtration, washed with 4 mL water and dried in a desiccator for 3 h. The complex $[(N4Py)Fe^{IV}(O)](PF_6)_2$ (**4**)[4] was obtained as blue solid in 68.5% yield (86 mg, 0.07 mmol). ^{1}H NMR (400 MHz, CD_3CN) δ (ppm) 44.12, 30.02, 9.70, 8.55, -10.49, -16.16, and -19.91.

$[(MeN4Py)Fe^{IV}(O)](PF_6)_2.2H_2O$ (2). Cerium ammonium nitrate (CAN) (339 mg, 0.62 mmol) in water (0.6 mL) was added to $[(MeN4Py)Fe^{II}(Cl)](Cl).2H_2O$ (160.8 mg, 0.28 mmol) in water (16 mL). A blue solid precipitated upon addition of aqueous KPF_6 (517 mg, 2.8 mmol in 4 mL water). The precipitate was recovered by vacuum filtration, washed with 4 mL of water and air-dried for 1 h. The complex $[(MeN4Py)Fe^{IV}(O)](PF_6)_2.2H_2O$ (**2**) was obtained as blue solid with 71% yield (178 mg, 0.24 mmol). ^{1}H NMR (400 MHz, CD_3CN) δ (ppm) 44.4, 30.7, 9.86, 8.5, -9.4, -12.76, -15.61 and -18.8. Anal. calc. for $C_{24}H_{23}N_5FeOP_2F_{12}$: C 38.8, H 3.12, N 9.42; Found: C 38.2, H 3.12, N 9.19.

Photochemistry Typical experiments used 2 mL of solution of **1 - 3** (0.125 mM) in the 1 cm pathlength cuvette. The light source was orthogonal to the monitoring beam of the UV-vis absorption spectrometer. LEDs (Thorlabs) were used at 365 nm (M365 F1, 6.10×10^{-5} einstein s^{-1} dm^{-3} or, for power dependent studies, M365LP1-C5, 1.19×10^{-5} einstein s^{-1} dm^{-3}), 490 nm (M490F3, 4.76×10^{-6} einstein s^{-1} dm^{-3}), 565 nm (M565F, 3.19×10^{-6} einstein s^{-1} dm^{-3}), 660 nm (M660F1, 4.0×10^{-6} einstein s^{-1} dm^{-3}), and 300 nm (M300F2, 1.25×10^{-6} einstein s^{-1} dm^{-3}) controlled by T-Cube Light Source & Driver Module (Thorlabs); or a DPSS laser at 355 nm (9.79×10^{-6} einstein s^{-1} dm^{-3}, Cobolt Lasers). For all irradiations, the power at the sample was measured with PM10V1 High Power 10 Watt sensor coupled to a FieldMate Power Meter.

Notes

‡ N4Py = (1,1-di(pyridin-2-yl)-N,N-bis(pyridin-2-ylmethyl)methanamine), MeN4Py = 1,1-di(pyridin-2-yl)-N,N-bis(pyridin-2-ylmethyl)ethan-1-amine, and BnTPEN = N-benzyl-N,N'N'-tris(2-pyridylmethyl)-1,2-diaminoethane

§ Complexes **2** and **3** show moderately higher rates of thermal reduction in CH_3CN than does **1**, but nevertheless photo-reduction to the corresponding Fe^{II} complexes upon irradiation at 365 nm proceeds substantially more rapidly than the thermal reactions in all cases.

§§ **1** oxidises methanol via α-C–H bond cleavage (HAT), manifested in a decrease in absorbance at 696 nm, increase in absorbance below 530 nm and the formation of formaldehyde. The thermal reaction between **1** and methanol at room temperature is essentially stopped by deuteration (CD_3OD) due to the large KIE (~ 50) for HAT.[17]

Caution. When working with perchlorate salts, suitable protective safeguards should be in place at all times due to the risk of explosion. Perchlorate salts should be handle in small (mg) quantities and used only where necessary.

2.5 Acknowledgements

We thank Dr. Apparao Draksharapu for help with the spectra analysis, Dr. Emma Harvey for GC measurements, and Dr. Waqas Rasheed for synthesis of complex **3**. The Ministry of Education, Culture and Science of the Netherlands (Gravity program 024.001.035, WRB), Ubbo Emmius fund (AD) and the Chinese Scholarship Council (JC) are acknowledged for financial support, as is the US National Science Foundation for work carried out in Minnesota (CHE1665391, LQ).

2.6 References

(1) Šima, J.; Makáňová, J. *Coord. Chem. Rev.* **1997**, *160*, 161–189.
(2) Allmand, A. J.; Webb, W. W. *J. Chem. Soc.* **1929**, No. 0, 1518–1531.
(3) Adamson, A. W.; Waltz, W. L.; Zinato, E.; Watts, D. W.; Fleischauer, P. D.; Lindholm, R. D. *Chem. Rev.* **1968**, *68* (5), 541–585.
(4) England, J.; Guo, Y.; Farquhar, E. R.; Young, V. G.; Münck, E.; Que, L. *J. Am. Chem. Soc.* **2010**, *132* (25), 8635–8644.
(5) Company, A.; Sabenya, G.; González-Béjar, M.; Gómez, L.; Clémancey, M.; Blondin, G.; Jasniewski, A. J.; Puri, M.; Browne, W. R.; Latour, J.-M.; Que, L.; Costas, M.; Pérez-Prieto, J.; Lloret-Fillol, J. *J. Am. Chem. Soc.* **2014**, *136* (12), 4624–4633.
(6) Kotani, H.; Suenobu, T.; Lee, Y.-M.; Nam, W.; Fukuzumi, S. *J. Am. Chem. Soc.* **2011**, *133* (10), 3249–3251.
(7) Kaizer, J.; Klinker, E. J.; Oh, N. Y.; Rohde, J. U.; Song, W. J.; Stubna, A.; Kim, J.; Münck, E.; Nam, W.; Que, L. *J. Am. Chem. Soc.* **2004**, *126* (2), 472–473.
(8) Hirao, H.; Kumar, D.; Que, L.; Shaik, S. *J. Am. Chem. Soc.* **2006**, *128* (26), 8590–8606.
(9) Draksharapu, A.; Li, Q.; Roelfes, G.; Browne, W. R. *Dalton Trans.* **2012**, *41* (42), 13180–13190.
(10) Draksharapu, A.; Li, Q.; Logtenberg, H.; van den Berg, T. A.; Meetsma, A.; Killeen, J. S.; Feringa, B. L.; Hage, R.; Roelfes, G.; Browne, W. R. *Inorg. Chem.* **2011**, *51* (2), 900–913.
(11) Oh, N. Y.; Suh, Y.; Park, M. J.; Seo, M. S.; Kim, J.; Nam, W. *Angew. Chemie Int. Ed.* **2005**, *44* (27), 4235–4239.
(12) Roelfes, G.; Lubben, M.; Chen, K.; Ho, R. Y. N.; Meetsma, A.; Genseberger, S.; Hermant, R. M.; Hage, R.; Mandai, S. K.; Young Jr., V. G.; Zang, Y.; Kooijman, H.; Spek, A. L.; Que Jr., L.; Feringa, B. L. *Inorg. Chem.* **1999**, *38* (8), 1929–1936.
(13) McDonald, A. R.; Que, L. *Coord. Chem. Rev.* **2013**, *257* (2), 414–428.
(14) Decker, A.; Rohde, J.-U.; Klinker, E. J.; Wong, S. D.; Que, L.; Solomon, E. I. *J. Am. Chem. Soc.*

2007, *129* (51), 15983–15996.

(15) Schenker, S.; Stein, P. C.; Wolny, J. A.; Brady, C.; McGarvey, J. J.; Toftlund, H.; Hauser, A. *Inorg. Chem.* 2001, *40* (1), 134–139.

(16) Lubben, M.; Meetsma, A.; Wilkinson, E. C.; Feringa, B.; Que, L. *Angew. Chemie Int. Ed. English* 1995, *34* (13–14), 1512–1514.

(17) Oh, N. Y.; Suh, Y.; Park, M. J.; Seo, M. S.; Kim, J.; Nam, W. *Angew. Chemie* 2005, *117* (27), 4307–4311.